Evaluation of a broadband marine source

Rob Telling[1*], Stuart Denny[1], Sergio Grion[1] and R. Gareth Williams[1] evaluate far-field signatures and compare processing results for a 2D test-line acquired with an experimental broadband source and a standard source.

The standard seismic air-gun array is a broadband source in the frequency range 2-200 Hz but the proximity of the sea-surface leads to interference between the direct down-going wave and its reflection from the surface. This interference manifests as peaks and notches in the spectrum that ultimately limit the bandwidth of available energy for processing and imaging. However, these notches are not perfect nulls and signal is still present above the noise (Williams and Pollatos, 2012). De-ghosting can recover the original bandwidth and improve the resolution and interpretability of the seismic section. The amount of signal recoverable from the notches depends on sea-state, noise level and scattering geometry: i.e. diversity of ray parameters contributing to an image. The signal level also depends on the acquisition set-up – receiver cable depth, source array depth and internal configuration.

In this paper we evaluate the potential of acquiring data using a source that seeks to minimize these ghost effects in the first place and preserve the original bandwidth. A standard seismic source array lies in a horizontal plane i.e. comprised of air-guns all at the same depth, so that all guns contribute to a single ghost response. However, it is possible to reduce the ensemble source ghost by placing guns at a range of depths within the array. This diversifies the frequencies at which the source ghost notch appears for each gun, leading to a flatter spectrum and, by appropriate timing of the guns, maintains the synchronized downward leading wave-front. This is not a new concept: the idea of placing source elements at different depths with timing delays was used in land acquisition at least as far back as the 1930s (see for example Prescott, 1935). Marine applications appear starting in the 1970s (see for example Cholet and Fail, 1970). Smith (1984) examined the technique in detail and is the precedent for all current work on multi-level air-gun arrays. While Parkes and Hegna (2011) and Siliqi et al. (2012), also make use of this source design principle, our study differs in the details of the processing and analysis of results. The standard source data we use as reference were processed up to the Nyquist frequency and not just up to the first source ghost notch frequency. Our objective is to compare the processing and source array solutions to the source ghost problem.

[1] *Dolphin Geophysical.*

[*] *Corresponding author, E-mail: rob.telling@dolphingeo.com*

Acquisition

Seismic data was acquired over a 30 km 2D sail-line in the Norwegian sector of the North Sea in November 2013 in a 20 knot northerly wind and 3 m sea-state. The acquisition parameters are summarized below:

- 1709 shots at 18.75 m spacing (854 standard source, 855 experimental source)
- Original shot spacing 18.75 m (37.5m shot interval for processing, after separation of sources)
- Standard source at 7 m depth, experimental source air-guns set at multiple depths
- Flat, hydrophone-only streamer, 30 m depth
- 640 receiver channels at 12.5 m spacing
- Near channel offset 150 m, far channel offset 8137.5 m
- 2 ms sample rate
- Record length 7.5 s

The standard and broadband source arrays comprised three strings each with six cluster positions and 28 guns in total, with guns ranging from 40 to 300 cubic inches. Total gun volume in each case was 4100 cubic inches. The air-guns in the standard array were all set at 7 m with identical timing. For the broadband source array the guns were deployed in a slanted configuration with depths ranging between 4.5 and 15.5 m to diversify the source ghosts and achieve a flatter spectrum. To ensure coherence of the positive peak of the downward propagating source wavelet, each gun in the broadband array was assigned a time delay, in the range 0.0 to 7.3 ms, based on its relative depth in the array. To minimize differences due to weather, water velocity and cable feathering, the data for both experimental source and standard source were acquired by firing shots alternately from each source along the same sail line. During the acquisition of the test line, the air-guns performed reliably, with no dropouts or significant timing errors.

Source

To characterize the two sources, we compare their far field signatures. The signatures were band-limited by a 2 Hz low-cut filter with 6 dB/octave slope and 214 Hz high-cut filter with 574 dB/octave. This is the same filter used during our acquisition experiment. The modelling assumed sea-water velocity 1500 m/s and calculated the ensemble response at a far field distance of 9 km. Figure 1 shows the vertical take-off modelled wavelets for the standard (conventional, flat) source and the experimental broadband source with and without sea-surface ghosts and Figure 2 shows the corresponding spectra. At vertical incidence, the first non-zero notch frequency appears at 107 Hz, corresponding to the condition for destructive interference between down-going phase-reversed reflected wave and direct down-going wave, with a path difference of twice the depth of the source array – in this case 7 m. Figure 3 shows the in-line directivity as a function of frequency. These plots illustrate the reduction in sea-surface ghost effect that can be achieved by diversifying the depths of guns within the array. As expected from a broadband source, no prominent notch frequencies are apparent in the ghosted broadband spectrum.

It is however important to point out that the source ghost creates not only an undesired destructive interference at the ghost notch frequency, but also constructive interference at frequencies away from the ghost notch: a broadband source attenuates both the destructive and the constructive interference. In terms of signal penetration, the broadband source provides a gain over the standard source in correspondence to the standard source's ghost notch frequencies, jointly with a loss at other frequencies. Figure 4 illustrates this concept. This figure shows the relative gain of the broadband source over the standard source, as a function of frequency. The blue curve is for vertical incidence, and the red curve for a 50° stack. The vertical incidence curve shows a considerable gain for the broadband source over the standard source in correspondence to the standard source ghost notch, and a corresponding loss for smaller and higher frequencies. In practice however, a seismic image is formed by stacking reflections from a variety of angles, and both

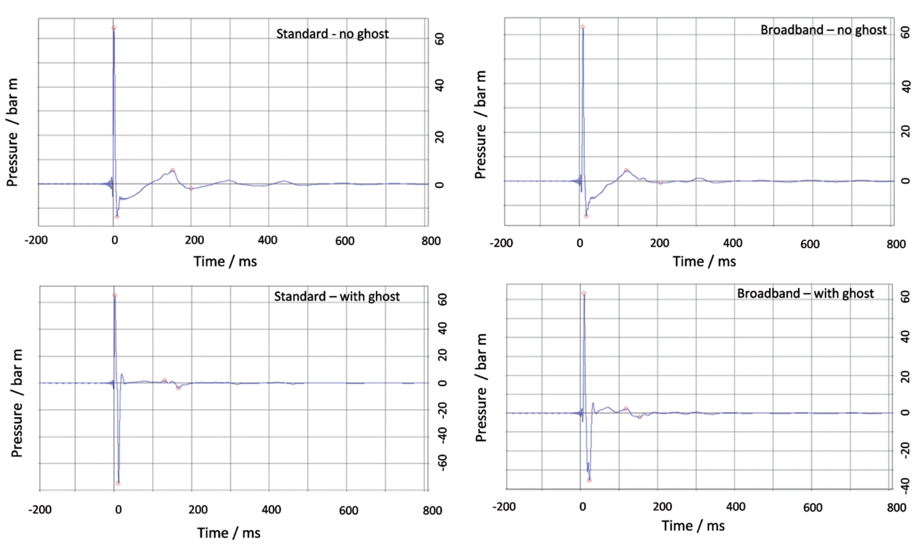

Figure 1 Typical ghost-free modelled source wavelet for standard (conventional) marine seismic air-gun array (top left) and with ghost due to sea-surface with reflection coefficient R = -1 (bottom left). Experimental broadband source modelled wavelet (top right) and corresponding wavelet with ghost (bottom right). Note the changes in scale.

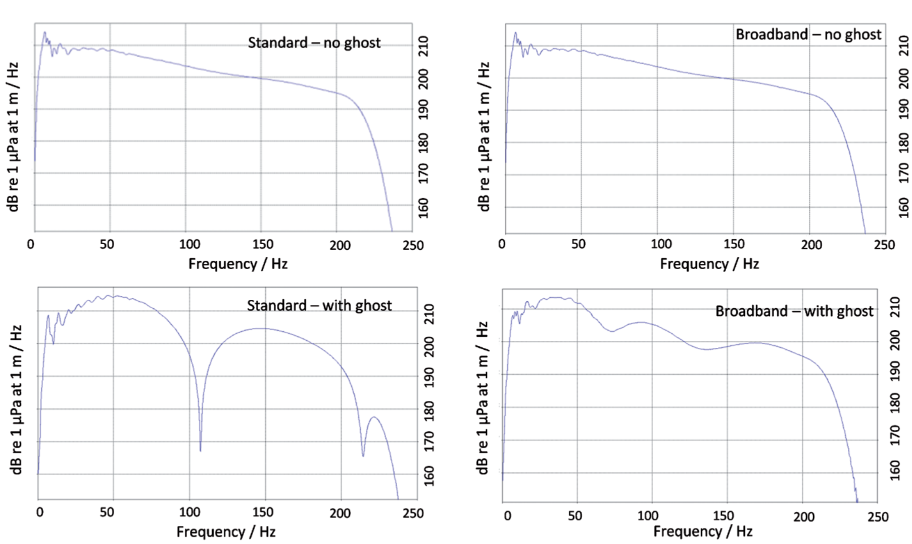

Figure 2 Ghost-free source modelled output spectrum for standard (conventional) marine seismic air-gun array (top left) and with ghost due to sea-surface with reflection coefficient R = -1 (bottom left). Experimental broadband source modelled output spectrum (top right) and corresponding spectrum with ghost (bottom right).

the source array response and the source ghost change with angle. For fully processed stacked data, the relative gain of the broadband over the standard source, in terms of energy penetration, is represented by the red curve in Figure 4. The theoretical stacked gain curve takes into account that during processing directional de-signature and velocity analysis and migration will tend to compensate for the amplitude and phase discrepancies due to source array directivity. For a 50° stack, the main expected advantage of the broadband source is in the range 90-180 Hz, as well as for frequencies below 40 Hz. For frequencies between 40 and 90 Hz, the broadband source contributes less energy to the stack than the standard source.

Modelling of the dropout stability of the two arrays indicated that the broadband source is more sensitive to dropouts, especially with time domain based criteria. Given the increased focus on spectral properties that has come with the advent of broadband acquisition, it may be more appropriate to specify dropout performance using spectral criteria.

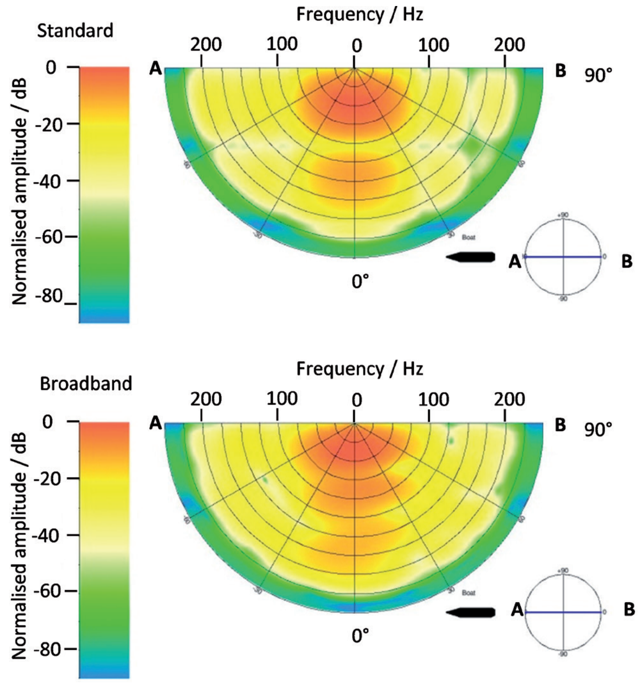

Figure 3 Array directivity as a function of in-line take-off angle and frequency for the standard (top image) and broadband source (bottom image).

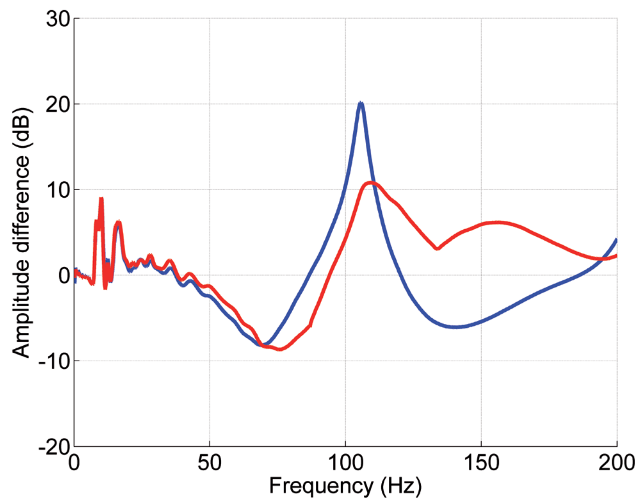

Figure 4 Relative gain of the broadband source over the standard source, at vertical incidence (blue) and for a 0° to 50° stack (red) as a function of frequency. The sea-surface reflection coefficient is R=-0.9.

Data processing

To ensure fair comparison, the datasets were processed using essentially identical pre-stack time migration sequences. An outline of the processing steps applied to the data is provided below:

- Field tape input; sort experimental and standard source records
- Fourier regularization of bad shot/channel edits
- 1.5 Hz/18 dB roll-off low-cut filter applied
- f-x swell noise attenuation
- Linear noise attenuation using f-k dip filter and removal of aliased energy
- De-convolution of bubble pulse and zero-phasing of wavelet
- Multiple attenuation by shallow-water-de-multiple, tau-p de-convolution and parabolic Radon de-multiple
- Source and receiver de-ghosting
- f-x de-convolution on binned common offsets
- Kirchhoff pre-stack time migration using picked 1 km velocity field
- Residual multiple attenuation using refined parabolic Radon de-multiple
- Residual noise attenuation, f-k filter, and time-varying low-pass filters
- Stack
- Amplitude, time and phase-matching of the different datasets

Bandwidth was preserved in the range 2-200 Hz by conservative low-cut filtering and for the high-frequency end, retaining a 2 ms sample interval. Swell noise attenuation was carried out in multiple iterations in both common shot and common channel sorts using f-x domain filtering. Linear noise from the direct arrival and tug/tail-buoy noise was attenuated using f-k dip filtering. Due to the shallow water it was not possible to extract a wavelet from the data; instead, bubble energy was attenuated using a de-convolution operator derived from the modelled far-field signature. Considerable energy from multiples was present in the data, most obviously being due to reverberation within the water-layer between sea-surface and sea-bed. The survey was in relatively shallow water (approximately 160 ms two-way travel time, equivalent to 120 m depth) which presented difficulties in using SRME effectively, due to missing near offset reflection data. Instead, a shallow-water multiple elimination algorithm was applied, using an operator derived from the shallower portion of data 0-2500 ms. This was followed by tau-p deconvolution to remove water-column reverberation apparent in the deeper parts of the data and finally, after a 1 km velocity pick, a parabolic Radon de-multiple process using time-varying move-out discrimination of primary and multiple.

The first step in source and receiver de-ghosting was performed on shot gathers transformed into the tau-p domain. This was followed by statistical corrections for minimization of residual ghost energy on common offset sections. The de-ghosting operators were time-space variant, derived using a combination of adaptive estimation and a-priori information on cable depth, source depth, water velocity and sea-surface reflection coefficient. Ghost delay time and the sea-surface reflection coefficient are thus treated as parameters to optimize in order to obtain the best attenuation of ghost. Source directivity (Figure 3 shows in-line directivity) is explicitly compensated for by directional de-convolution in the de-ghosting process using far-field signatures with and without ghosts modelled at 1 degree angle intervals. Apart from the different source de-ghosting operators, processing parameters for both datasets were kept the same. Pre-stack time migration was carried out using a Kirchhoff operator and smoothed in a 1 km picked velocity field with a maximum aperture of 5 km and 50 degree dip angle limit. Following a second Radon de-multiple sequence, residual noise attenuation was applied to common offset sections and the data stacked. As a final processing step, the broadband source stack was matched to the standard source stack to remove any small residual bulk time, amplitude and phase shifts.

Results

Firstly, a comparison was made of the effect of processing the standard source data over the full available bandwidth 2-200 Hz with processing only up to the first source notch 2-107 Hz. Figure 5 shows a shallow section of the data, where the greatest increase in resolution is expected. The arrows in the figure highlight some of the horizons that are resolved with full bandwidth available but which are not visible or poorly resolved for the band-limited case.

The fully-processed sections obtained with the broadband source and using the standard source, together with a difference section were then examined in detail. These sections are shown in Figure 6. Note that, because of the acquisition configuration, the two lines have adjacent but not coincident imaging mid-points and therefore the datasets are not identical, and are most dissimilar at the sea-floor – hence its prominence in the difference section. However, these two sections appear broadly comparable, from a structural imaging point of view. This overall similarity in appearance is due to the processing effort in attenuating ghost arrivals in both datasets, as well as to the noise and multiple attenuation sequences. Frequency-dependent differences are not easily identifiable in the broadband stacked sections. To investigate the relative merits of the two datasets further, and taking into account the relative gain curves in Figure 4, we now focus on the

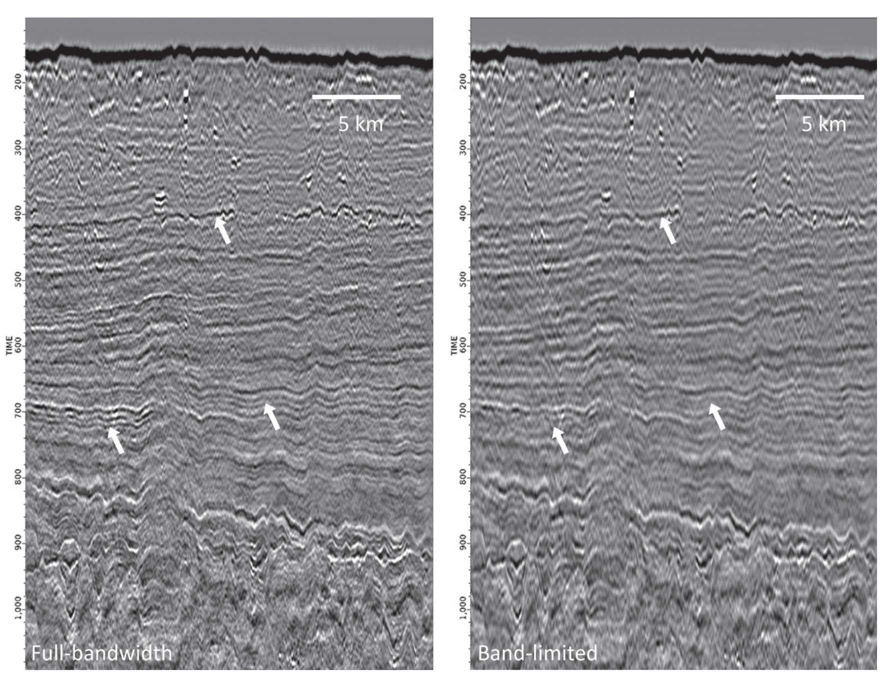

Figure 5 *Standard source sections: full-bandwidth (left) and band-limited by source notch (right).*

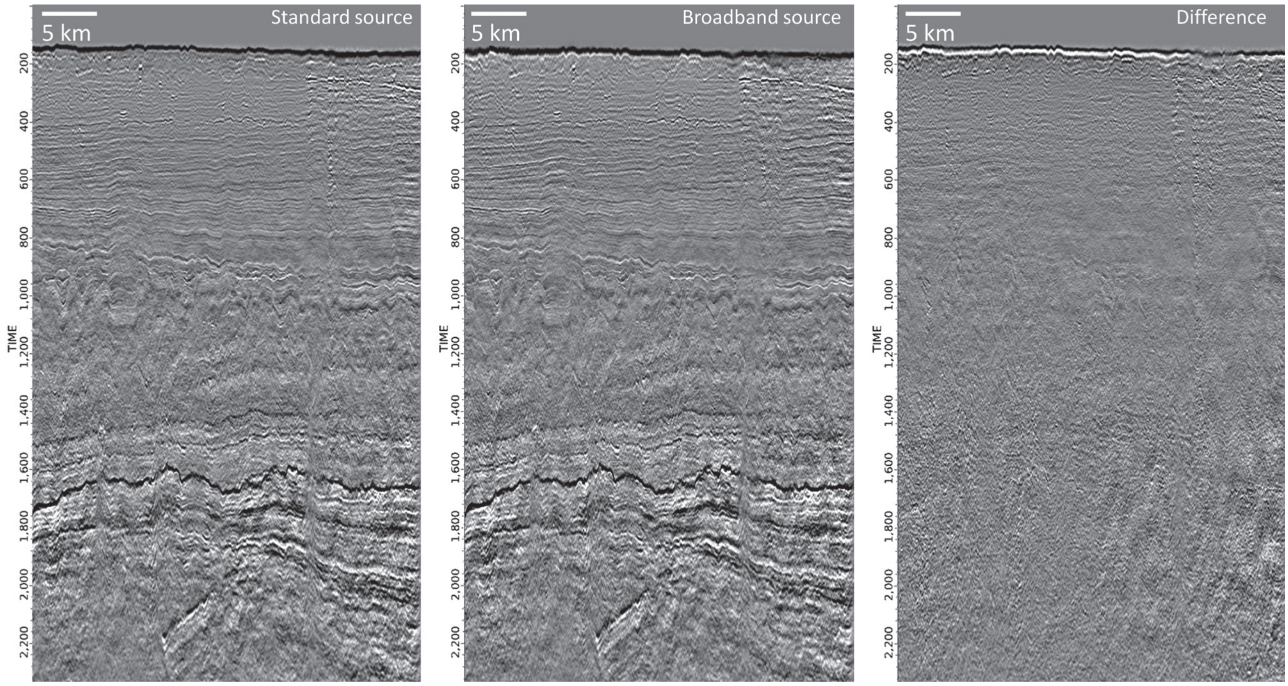

Figure 6 *Sections obtained using standard source (left), broadband source (centre) and difference (right).*

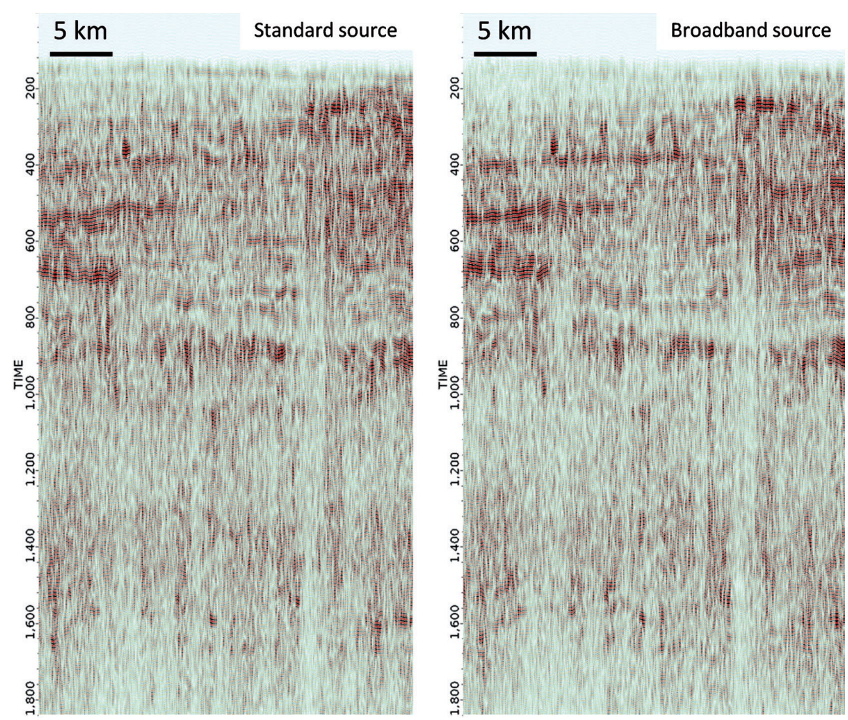

Figure 7 *Standard (left) and broadband source (right) in a 10 Hz band centred on 107 Hz i.e. the standard source ghost notch.*

frequency range where the greatest difference between the datasets is expected. We apply a narrow 102-112 Hz band-pass filter to the data, with a roll-off of 72 dB/octave. These filtered datasets are shown in Figure 7. The narrow-band view highlights qualitatively the improvement that is obtained with the broadband source – this being greater lateral coherence and signal strength for events in the shallow data.

To quantify this small improvement in the 102-112 Hz band and extend the analysis of the two datasets over the whole frequency range, a signal-to-noise (SNR) ratio estimate was derived. The SNR estimate is based on the predictability attribute P between two traces A and B, as defined for example in Kragh and Christie (2002) in the context of time-lapse repeatability analysis:

$$P = \frac{\Sigma\Phi_{AB}(\tau)\Phi_{AB}(\tau)}{\Sigma\Phi_{AA}(\tau)\Phi_{BB}(\tau)} \tag{1}$$

where Φ_{AB} is the cross-correlation between A and B, Φ_{AA} is the autocorrelation, and the calculation is carried out over a range of lags τ. A signal to noise ratio estimate can then be obtained as

$$SNR = \frac{1}{\sqrt{\frac{1}{P} - 1}} \tag{2}$$

We calculate the SNR for the standard and broadband datasets individually, by applying equation (2) to each trace A and an adjacent trace B at a distance X from A, in 10 Hz bands. More in detail, we considered trace distances from 6.25 to 300 m, and averaged the corresponding results. Additionally, for our analysis, we used eight positive and negative time lags to allow for the presence of geological structures with a variety of geological dips.

In order to compare the broadband source and standard source datasets, we then take the difference between the SNR estimates expressed in dB. The result is shown in Figure 8 in blue for a stack of raw data and in red for the fully processed images. Also shown are the statistical error bars for the two estimates, one every 30 Hz. This analysis confirms the qualitative assessment that standard and broadband source datasets are very similar, as the differences rarely exceed 1 dB. For the raw data, the relative SNR gain curve shows alternating peaks and troughs that resemble in location those shown in Figure 4 for the vertical incidence case, and can be attributed to the different performance of the two sources in different frequency bands. It should be pointed out however, that this SNR estimate is subject to pitfalls: for example, its reliability tends to decrease with increasing frequency, in particular for increasing geological complexity. This may explain why the 10 dB peak at around 110 Hz in Figure 4 corresponds to a more modest 0.5 dB in Figure 8. The fact that the SNR of the fully processed data is less variable than for the raw data shows that processing is capable of reducing the SNR discrepancies that arise from the different nature of the two sources, and also matches a similar observation on the theoretical vertical incidence and stacked curves of Figure 4. There appears to be a modest advantage for the broadband source data over the standard data of the order of 0.5 to 1 dB in the band 50-150 Hz, in agreement with the qualitative comparison of Figure 7 and broader, although less pronounced, than the gain predicted in Figure 4. In terms of low frequencies, the 2-2.5dB gain of the broadband source over the standard in the raw data appears to have been equalized by our processing sequence.

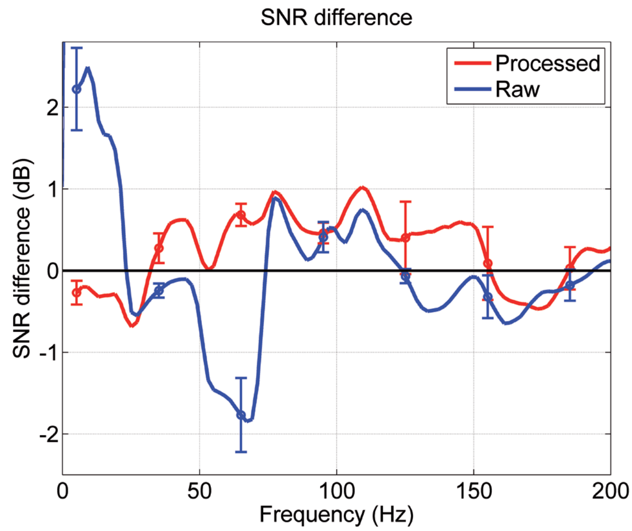

***Figure 8** Estimated SNR difference between broadband and standard source datasets, as a function of frequency for raw data stack (blue) and processed data stack (red).*

Discussion

The first point to note, which is apparent from Figure 5, is the clear improvement in imaging, particularly for two-way travel times up to 1500 ms, that is afforded by recovering the bandwidth beyond the standard source first ghost notch and processing up to 200 Hz. This advantage, in terms of higher temporal resolution in the wavelet, will hold for whichever source type is used in acquisition. The stacked data shows horizons in the shallow (0-1000 ms) that are well-resolved with the full available bandwidth and that are not visible using the conventional approach of cutting at or just below the frequency of first source ghost notch.

The second point to note, which is best illustrated by Figure 7 and Figure 8, is that the signal-to-noise ratio after full processing is marginally higher for the broadband source when compared with the standard source. The signal, in the form of coherent energy that tracks geological horizons, is present for both source types but the lateral coherency is higher for the broadband source. This difference is most apparent around the band where the first notch appears due to the source ghost, but is relatively small. This implies that the recovery of signal bandwidth from the standard source, after source de-ghosting, is effective. In practice the advantage offered by the broadband source, being primarily at high frequency, will be for high-resolution imaging of shallow geology. For example, in this survey the signal in the band 102-112 Hz was observable down to approximately 1000 ms.

A preliminary evaluation of the stability of the two sources was conducted based on the near field hydrophone recordings made during the test line. Both sources exhibited good stability in the band 15-140 Hz, with lower stability outside this band, and with the exception that the standard source exhibited reduced stability at the source ghost notch.

Conclusions

This work has demonstrated that there are advantages in extending conventional source bandwidth through processing, and that modest additional benefit, in terms of signal-to-noise ratio can be achieved when using a multi-level broadband source. For the dataset used in this study, the effects due to interaction with the sea surface were successfully minimized, generating a relatively high and uniform signal level across the frequency range 2-200 Hz. When the broadband source data is compared to that acquired using a standard source, signal-to-noise ratio is slightly higher and this improves image quality in the shallow data.

Acknowledgements

The data shown are provided courtesy of Dolphin's Multi-Client Department.

References

Cholet, J. and Fail, J. [1970] *System for Seismic Prospecting in Water*. United Kingdom Patent 1,193, 507.

Kragh, E. and Christie, P. [2012] Seismic repeatability, normalized rms, and predictability. *The Leading Edge*, 640-647.

Parkes, G. and Hegna, S. [2011] A marine seismic acquisition system that provides a full 'ghost-free' solution. *SEG 81st Annual International Meeting*, Expanded abstracts, 37-41.

Prescott, H. [1935] *Method of Making Geological Explorations*. United States Patent 1, 998, 412.

Siliqi, R., Payen T., Sablon, R. and Desrues, K. [2012] Synchronized multi-level source, a robust broadband marine solution. *SEG 82nd Annual International Meeting*, Expanded Abstracts, 56-60.

Smith, G. [1984] Three Dimensional Air Gun Arrays. *SEG 54th Annual International Meeting*, Expanded abstracts, 282-285.

Williams, R.G. and Pollatos, J. [2012] Signal to noise - the key to increased marine seismic bandwidth. *First Break*, **30** (11), 101 105.